Tropical cirrus clouds near cold point tropopause under ice supersaturated conditions observed by lidar and balloon-borne cryogenic frost point hygrometer

Takashi Shibata,[1] Holger Vömel,[2] Saipul Hamdi,[3] Sri Kaloka,[3] Fumio Hasebe,[4] Masatomo Fujiwara,[4] and Masato Shiotani[5]

Received 3 April 2006; revised 17 August 2006; accepted 20 September 2006; published 13 February 2007.

[1] Simultaneous vertical profiles of cirrus cloud backscattering and frost point temperature were obtained for the first time in the tropopause region over Bandung, Indonesia, (6.9°S, 107.6°E). These profiles were measured by ground-based lidar and by balloon-borne Cryogenic Frost point Hygrometer (CFH) sondes. Supersaturation up to several ten percent was observed by the CFH just below the cold point tropopause at the altitude where a cirrus cloud was observed by lidar. The water vapor mixing ratio decreased slightly at the altitude of the cirrus cloud, suggesting that this decrease was caused by uptake in the cirrus cloud and that the water vapor reduction corresponds to the lower limit of the cloud water content of the observed cirrus cloud. Theoretical calculations of the scattering parameters for the observed cirrus cloud particles and estimations of the time constants for sedimentation and for condensational growth indicate that particles size range is between 4 μm and 30 μm.

Citation: Shibata, T., H. Vömel, S. Hamdi, S. Kaloka, F. Hasebe, M. Fujiwara, and M. Shiotani (2007), Tropical cirrus clouds near cold point tropopause under ice supersaturated conditions observed by lidar and balloon-borne cryogenic frost point hygrometer, *J. Geophys. Res.*, *112*, D03210, doi:10.1029/2006JD007361.

1. Introduction

[2] Optically thin cirrus clouds near the tropopause, ubiquitous throughout the tropical region [*Wang et al.*, 1996; *Winker and Trepte*, 1998; *Dessler et al.*, 2006], are often referred to as subvisual cirrus clouds (SVC) because they are visually undetectable [*Lynch and Sassen*, 2002]. The appearance of these clouds is closely related to the transport of water from the troposphere to the stratosphere and the dehydration processes in the tropical tropopause layer (TTL) [*Jensen et al.*, 1996a; *Rosenfield et al.*, 1998; *Vömel et al.*, 2002]. Since these thin cirrus clouds cover a wide area of the tropical tropopause, they influence the global climate through radiative processes [*Wang et al.*, 1996; *Jensen et al.*, 1996b; *Boehm et al.*, 1999] and influence the vertical transport through the TTL [*Corti et al.*, 2006].

[3] Thin cirrus clouds are very frequently observed in the tropics, even in areas without local convective activity [*Winker and Trepte*, 1998]. *Boehm et al.* [1999] examined the mechanisms that maintain these clouds using a two-dimensional numerical cloud-resolving model. They concluded that large-scale upward motion is needed to maintain the clouds. Furthermore, they suggested that a mechanism that slows the evaporation by reducing the equilibrium vapor pressure would be effective in maintaining the clouds. *Luo et al.* [2003] proposed another mechanism that stabilizes the vertical structure of the observed ultrathin tropical tropopause clouds [*Peter et al.*, 2003]. This mechanism requires that the relative humidity over ice is about 100% at the cloud base, increasing with altitude, and that the vertical wind velocity decreases with the altitude.

[4] Although the existence of cirrus clouds at subsaturated conditions was suggested by *Boehm et al.* [1999], there are several observations by airborne hygrometers of supersaturation over ice in cirrus clouds [e.g., *Jensen et al.*, 1998, 1999, 2005a; *Gierens et al.*, 2000; *Ovarlez et al.*, 2002; *Luo et al.*, 2003; *Gao et al.*, 2004].

[5] In spite of many studies of tropical thin cirrus clouds, the dynamical and microphysical processes within cirrus clouds are still not clear. Furthermore, although cirrus clouds have been frequently observed, these observations often provide only snapshots. Satellite observations often detect the presence of cirrus clouds near and below the tropical tropopause. However, the spatial resolution of the observations is low, and the observations usually lack simultaneous temperature and water vapor measurements. Airborne instruments can measure cloud particles, trace gases and dynamical parameters simultaneously, but are limited in time and region by the high operating costs for

[1]Graduate School of Environmental Studies, Nagoya University, Nagoya, Japan.
[2]Cooperative Institute for Research in Environmental Sciences, University of Colorado, Boulder, Colorado, USA.
[3]Lembaga Penerbangan dan Antariksa Nasional, Bandung, Indonesia.
[4]Faculty of Environmental Earth Science, Hokkaido University, Sapporo, Japan.
[5]Research Institute for Sustainable Humanosphere, Kyoto University, Kyoto, Japan.

0148-0227/07/2006JD007361

research aircrafts. Furthermore, temperature and pressure measurements onboard fast aircrafts need large corrections that might significantly influence the interpretation [*Murphy*, 2005]. Some ground based lidar observations of tropical tropopause cirrus have been reported, but lacked simultaneous water vapor observations.

[6] Although supersaturation in cirrus clouds has been reported, the details of the vertical structure of cirrus clouds by lidar and of water vapor by balloon-borne hygrometer have not yet been simultaneously obtained. Continuous observations of cirrus clouds by ground based lidar combined with accurate humidity observations by balloon-borne hygrometers will enhance the understanding of cirrus cloud processes near the tropical tropopause. We conducted observations of cirrus clouds using a Mie lidar system at Bandung, Indonesia, (6.9°S, 107.6°E) to study their properties as function of altitude. The lidar tuning has been optimized for cirrus cloud observations in the tropical tropopause region. For accurate humidity measurements in the upper troposphere and lower stratosphere we used the balloon-borne Cryogenic Frost point Hygrometer (CFH), which is a new development based on the well established NOAA/CMDL frost point hygrometer [*Vömel et al.*, 1995, 2006]. The first simultaneous CFH/lidar observations were conducted in Indonesia to study the relation between cirrus clouds and humidity near the tropical tropopause.

[7] It is widely recognized that the tropical tropopause is not a simple boundary separating the troposphere and the stratosphere; instead, it should be regarded as a layer that has both tropospheric and stratospheric characteristics [*Attics and Robinson*, 1983; *Highwood and Hoskins*, 1998; *Folkins et al.*, 1999]. Cirrus clouds are frequently observed in the tropical tropopause layer (TTL) and may indicate dehydration processes in the tropopause region [e.g., *Holton and Gettelman*, 2001]. Indonesia is in the outflow of the region of the coldest tropopause temperatures over the western Pacific. Dehydrated or still dehydrating air and simultaneously the corresponding clouds that are a result of the dehydration process can be observed over Indonesia.

[8] In the following sections, we present results of the first simultaneous lidar and CFH observations. In section 2, the instruments used in the observations are briefly described. In section 3, the general features of the observed results are highlighted. In section 4, the size of the cirrus cloud particles is estimated, and the implications of the observations are discussed.

2. Instruments

2.1. Mie Lidar

[9] The lidar is a Nd:YAG laser-based Mie scattering depolarization lidar. Only the second harmonic wavelength (532 nm) of the laser is used for the observations. The lidar detects two polarization components of the backscatter signal, which are parallel and perpendicular to the polarization plane of the linearly polarized transmitted laser pulse. The diameter of the receiving telescope is 20 cm and the field of view is 0.5 mrad. The relatively small field of view reduces background noise, and makes the multiple scattered signals from optically thin cirrus clouds negligible. The bandwidth of the interference filter is 0.3 nm (FWHM). The signals from the detectors (photomultiplier tubes) are processed by 12-bit transient recorders. The vertical resolution of the lidar data is 15 m and the integration time of the data is 30 s.

[10] The backscattering ratio R is defined as

$$R(z) = \frac{B_R(z) + B(z)}{B_R(z)}, \tag{1}$$

where B_R and B are the backscattering coefficients corresponding to Rayleigh scattering from atmospheric molecules and to Mie scattering from cloud particles, respectively. The backscattering ratio minus one $(R-1)$ is roughly proportional to the mass-mixing ratio of the cloud particles. B is calculated as $B_R(R-1)$. The detection limit of the optical thickness of cirrus cloud near tropical tropopause is estimated to be less than about 10^{-4}, although the limit depends greatly on the sky conditions.

[11] The depolarization ratio D is defined as

$$D(z) = \frac{B_s(z)}{B_p(z) + B_s(z)}, \tag{2}$$

where B_p and B_s are the parallel and perpendicular components of the Mie (and Rayleigh) backscattering coefficients, respectively. The depolarization by Rayleigh scattering can be ignored since it is less than 1% of the depolarization by Mie scattering from cirrus clouds. For liquid cloud particles or spherical particles, D is equal to zero. For randomly oriented cirrus cloud particles, D has a value of about 0.3, which will be explained below.

2.2. Balloon Payload

[12] The payload consists of the CFH, an electrochemical concentration cell (ECC) ozonesonde, a Vaisala RS80 radiosonde, and the GPS and was launched using small rubber balloons. The CFH measures the temperature of a small frost layer that is kept in equilibrium with the atmospheric water vapor, which is by definition the frost point temperature. The frost point measurement is not affected by cloud particles while the CFH is in cirrus clouds. A detailed description of the CFH can be found in the paper by *Vömel et al.* [2006]. The vapor pressure is calculated from the measured frost point temperature using the equation by *Goff and Gratch* [1946] and the relative humidity (RH) is calculated from the vapor pressure and the Vaisala RS80 temperature measurement. Throughout the paper RH and supersaturation refer to relative humidity over ice (RHi). The GPS provides the position of the balloon, and wind information.

3. Results of Simultaneous Lidar and CFH Observations in December 2004

3.1. Cirrus Clouds and RHi Observations

[13] In December 2004, four CFH water vapor/ECC ozone payloads were launched at Bandung, Indonesia. During this period the lidar was operating almost continuously. Although lidar observations in the tropopause region were often interrupted by dense lower level clouds, which are common during the rainy season, lidar profiles in the tropopause region were obtained during the CFH soundings on 15 and 16 December. Figure 1 shows the time-height

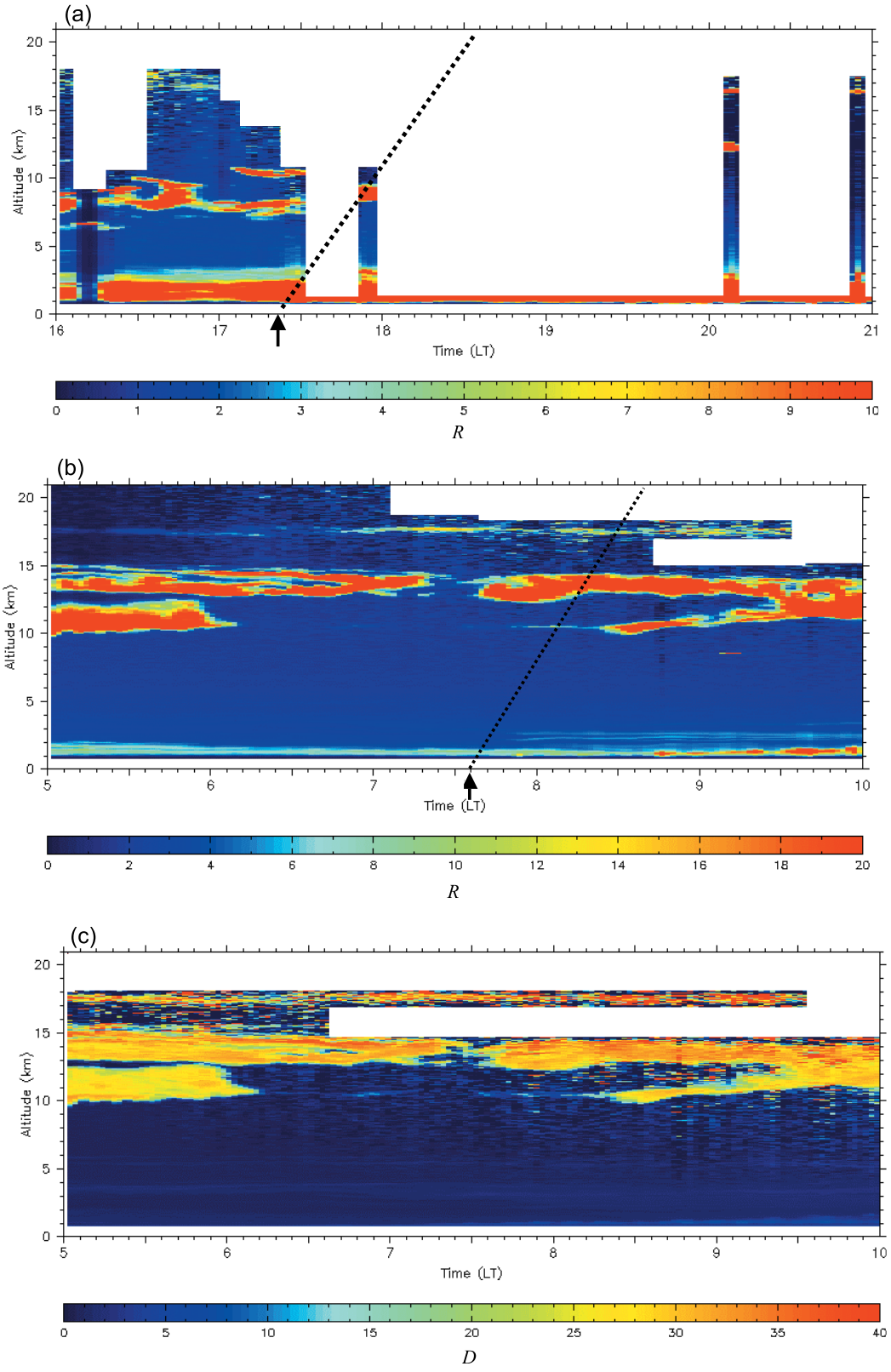

Figure 1. (a) Time-height cross section of the scattering ratio R during the evening of 15 December 2004. Regions with poor data quality are masked. The arrow shows the time of balloon launching. The dotted line shows the approximate time and altitude of CFH. (b) Time-height cross section of the scattering ratio R during the morning of 16 December 2004. Regions with poor data quality are masked. The arrow indicates the balloon launch. The dotted line shows the approximate time and altitude of the CFH. (c) Time-height cross section of the depolarization ratio D during the morning of 16 December 2004. Regions with poor data quality are masked.

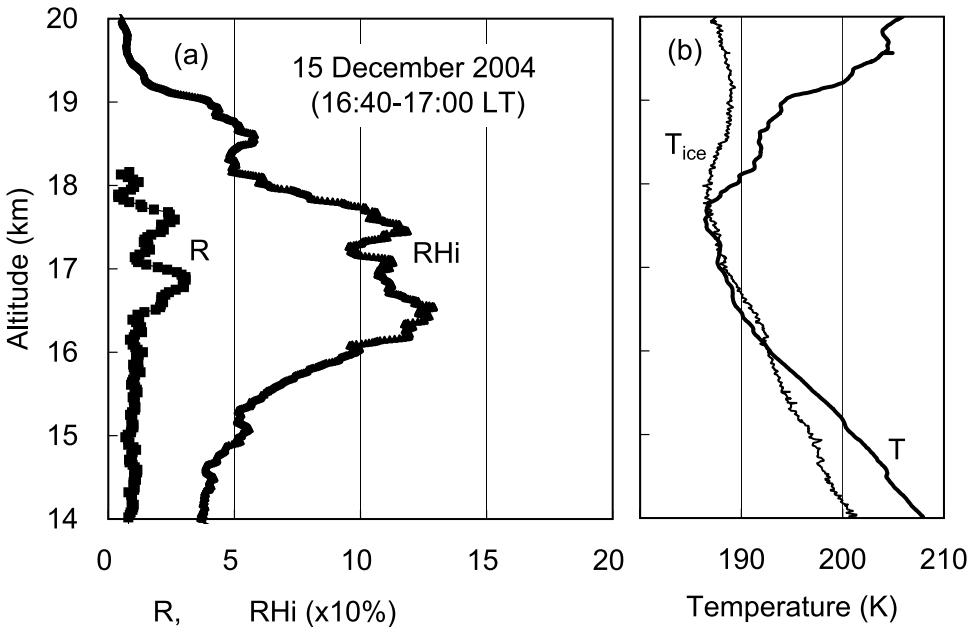

Figure 2. (a) Scattering ratio (R) from lidar observations and relative humidity (RHi) from CFH observations in the evening of 15 December 2004. (b) Ambient temperature (T) and frost point temperature (T_{ice}).

cross sections of the backscattering ratio (R) observed on 15 December and on 16 December, as well as the depolarization ratio (D) observed on 16 December 2004, respectively. The CFH sondes were launched at 1722 local time (LT) on the 15 December and at 0736 LT on 16 December, respectively. In Figure 1, the approximate time and height of the CFH observations are indicated by dotted lines.

[14] Figures 2 and 3 show the profiles of the scattering ratio R, RHi, ambient temperature, and frost point temperature. In Figure 3, RHi and frost point temperature are only shown where the CFH gave reliable data. Although low level clouds persisted from the afternoon of 15 December to the early morning of 16 December (Figure 1a), cirrus clouds around 17 km were detected during short periods when the lower level clouds allowed penetration of the lidar signal. In Figures 1b and 3a, cirrus clouds are clearly seen between 17.2 and 17.8 km from 0530 to 0930 LT on 16 December. These clouds were just below the cold point tropopause

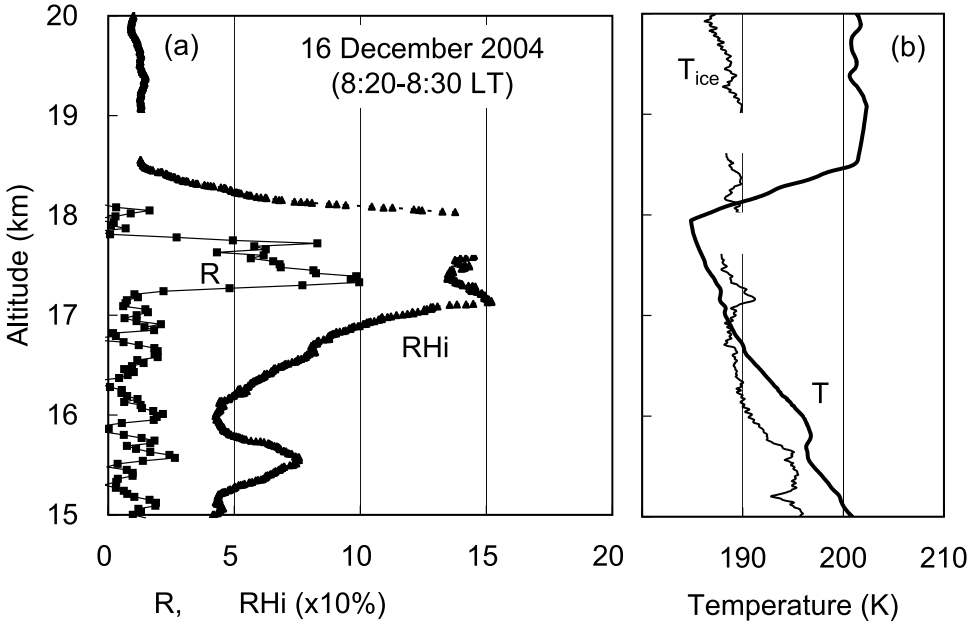

Figure 3. (a) Scattering ratio (R) from lidar observations and relative humidity (RHi) from CFH observations in the morning of 16 December 2004. (b) Ambient temperature (T) and frost point temperature (T_{ice}).

(CPT) at 17.9 km. Throughout this altitude range the depolarization ratio of the cirrus clouds is around 30–40% (Figure 1c).

[15] Both RHi profiles on 15 and 16 December (Figures 2a and 3a) were taken during the balloon ascent. The profiles show supersaturation between 16.2 km and 17.7 km on 15 December, and between 16.8 km and 18.1 km on 16 December.

3.2. Comparison Between the Lidar and CFH Observations

[16] On 15 December 2004, the CFH reached 17 km at 1820 LT. The backscattering ratio R in Figure 2a was taken from lidar data between 1640 and 1700 LT, because lidar observations were not possible at the time of the CFH observations because of dense low level clouds. Cirrus clouds were detected between 16.5 km and 17.7 km (Figure 2a), showing two distinct maxima of R with values of 3 and 2 at 16.8 km and 17.6 km respectively. The RHi measurements showed supersaturation between 16.2 and 17.7 km with two distinct maxima of 130% and 120% at 16.5 km and 17.6 km respectively. The lower supersaturation peak was observed in cloud free air just below the cirrus cloud.

[17] In the morning of 16 December, the CFH passed 15 km to 18 km between 0820 and 0830 LT (Figure 3a) with the lidar observations taking place at the same time. Cirrus clouds were observed between 17.2 km and 17.8 km with a maximum scattering ratio of 10 at 17.4 km. The RHi profile showed supersaturation between 16.8 km and 18.1 km, with a maximum value of 160% at 17.2 km. Again, the supersaturation peak was observed in particle free air just below the cirrus cloud, and the layer of supersaturation encompasses the entire cirrus cloud.

[18] We should pay attention to another feature in the observed RHi profile: The humidity decreased slightly at the altitudes where the cirrus clouds were observed (16.7–17.6 km on 15 December, and 17.3–17.6 on 16 December). This may be evidence for water vapor uptake by the cloud. Since water vapor is reduced by the formation and growth of the clouds particles, the decrease in the humidity profiles at the altitudes of the cirrus clouds suggests that it was caused by the condensation of water vapor due to the growth of the cloud particles. If this is the case, the amount of water vapor decrease should correspond to the ice water content of the cloud.

4. Discussions

4.1. Cloud Water Content and Ice Crystal Size

[19] The size of cirrus cloud particles is one of the most fundamental parameters for understanding their microphysical properties and for estimating their radiative effects. Since the lidar uses only one wavelength to detect cirrus clouds, it is not possible to retrieve any size information of the cloud particles from the backscattering coefficient alone. However, if the water vapor decrease corresponded to the ice water content of the cloud particles as suggested above, we could then use this information together with the backscattering coefficient to estimate the cloud particle size. For this, we use the data taken on 16 December since lidar and CFH observations were made almost simultaneously. The estimating size has another consequence: It makes it possible to determine the validity of the suggested relation between the decrease in water vapor and the ice water content by checking whether the estimated size is realistic.

[20] To estimate the amount of water vapor loss, we need to know the reference level for this loss. Since the nucleation threshold for cloud particles will be at some critical value of supersaturation, we assume that the reference level is at the observed maximum of relative humidity, with the assumption that ice particles nucleated at an RHi value similar to that observed maximum. The sounding on 16 December shows an RHi maximum in cloud free air, which can be used to estimate the lower limit of the water vapor loss, which corresponds to the cloud water content (cwc). The maximum value of RHi is 152% at an altitude of 17.1 km. The temperature at this altitude is 188 K. *Koop et al.* [2000] estimated ice-nucleation-threshold-RHi as a function of temperature. Their estimated threshold RHi for 188 K is 160–165%, which is about 10% larger than observed maximum RHi (152%). Considering the large uncertainty in theoretical estimation of a nucleation ratio, we can think that these values agree very well. Using the backscattering coefficient B, we can calculate the ratio of cwc/B. This ratio is directly related to the cloud particle radius (described below).

[21] Figure 4a shows the water vapor mixing ratio and the humidity for the sounding on 16 December. Figure 4b shows the backscattering coefficient B (/m·sr) measured during this sounding. The RHi maximum is indicated by the short vertical line and the water vapor loss was taken as the difference between the observed RHi and this level (hatched area). Figure 4c shows the relation between the RHi and B shown in Figures 4a and 4b for the height range of the hatched area. RHi and B are negatively correlated in this height range, with a correlation coefficient of -0.90. The ratio cwc/B was calculated for the altitude range between 17.2 km and 17.6 km. Its mean value for this layer is 23 g sr/m^2. Figure 4a also shows the cloud water content, which was calculated by multiplying the measured backscatter coefficient B by this value.

[22] With this estimation of cwc/B and the assumptions above we can estimate the size of the cirrus cloud particles from geometrical scattering calculations as described in Appendix A1. These calculations allow a theoretical estimation of cwc/B, the depolarization ratio (D), and the cirrus cloud particle number concentration divided by the backscattering coefficient (N/B) as a function of particle size, which are shown in Figure 5. The abscissa of Figure 5 shows the effective radii, which is defined as the radius of a sphere whose surface area is four times the average cross section of randomly oriented hexagonal ice columns. The effective radius of the crystal has an approximately linear relationship with cwc/B because cwc is proportional to the volume and B is proportional to the cross section of the particles. As a result of this calculation we can estimate the particle size from the estimated value of cwc/B. Figure 5 shows that a cwc/B value of 23 gsr/m^2 corresponds to an effective radius of about 5 μm.

[23] The theoretically calculated depolarization ratio shown in Figure 5 is nearly constant at a value of 30–33% over the range of particles sizes, which agrees well with the observed values shown in Figure 1c. The value for N/B (number concentration divided by backscattering coef-

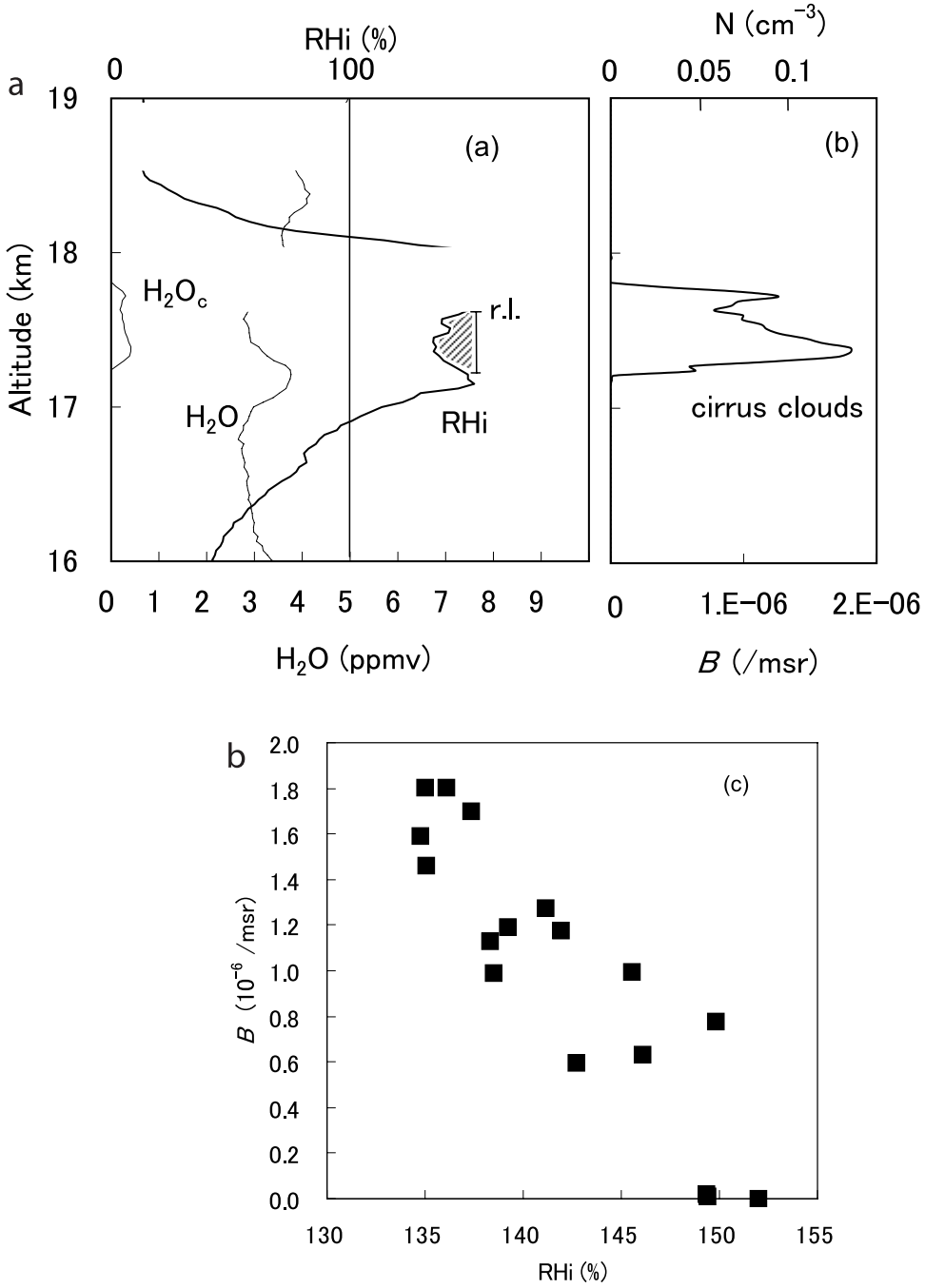

Figure 4. (a) Profiles of water mixing ratios: gas phase from CFH observations(thin line; H_2O), condensed phase from the lidar observations (thin line; H_2O_c); and relative humidity over ice (solid line; RHi). The water vapor reference level is indicated by the vertical line (r.l.). The hatched area is assumed as the lower limit of the water vapor decrease. (b) Backscattering coefficient (B). (c) Correlation between RHi and B at altitude range of hatched area in Figure 4a. The correlation coefficient between RHi and B is −0.90.

ficient) at a radius of 5 μm is about 7.5×10^4 msr/cm^3. The scale for the number concentration (upper abscissa of Figure 4b) was calculated from this value for N/B. Since N/B decreases with radius (except at the smallest size range), this number concentration corresponds to an upper limit.

[24] Lidar and CFH observed cirrus clouds and water vapor simultaneously, but they did not observe exactly the same air mass. The distance between the lidar and the launch site is only about 30 m. However, the balloons do not ascent in a vertical straight line, but rather drift with the horizontal winds during ascent and descent. When the balloon reached the tropopause, the horizontal separation between lidar and balloon was given by the GPS onboard the balloon payload. It was 15 km

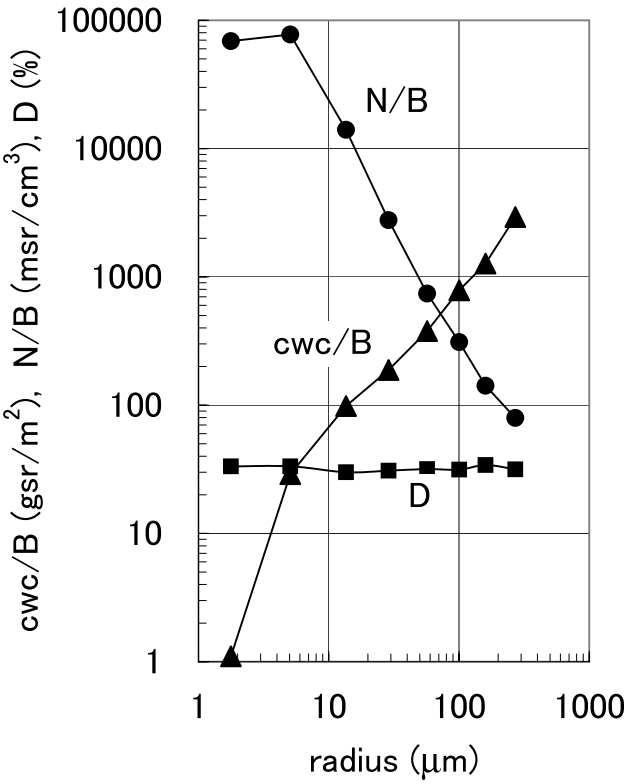

Figure 5. Theoretically calculated cwc/B versus the effective radius, depolarization ratio (D), and cirrus cloud particle number concentration (N) divided by B.

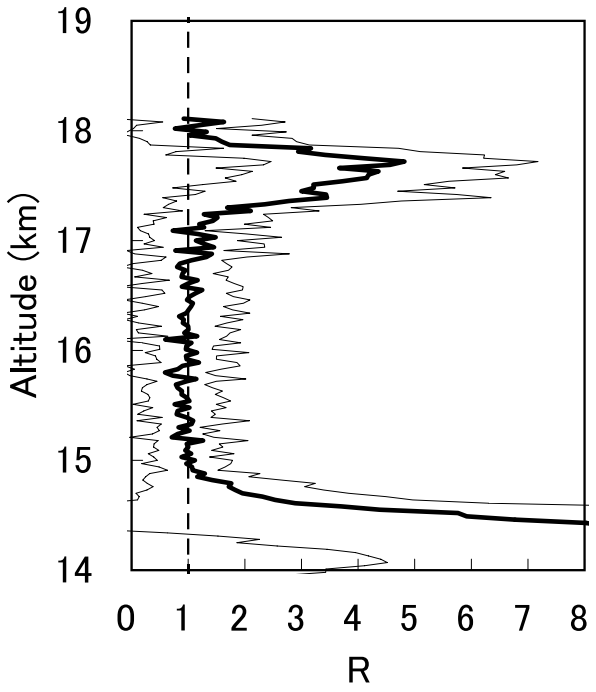

Figure 6. Averaged scattering ratio profile (R; bold line), and its standard deviation (thin lines) observed between 0600 and 0900 LT on 16 December.

for the sounding on 15 December and 20 km for the sounding on 16 December.

[25] Although the altitude range of the cirrus clouds was very stable, the scattering ratio R and the backscattering coefficient B were quite variable. Figure 6 shows the average and the standard deviation for the scattering ratio observed between 0600 and 0900 LT on 16 December. The relative variation of $R-1$ (or B) is about 100%. B showed variations from roughly one tenth to twice the observed value. Assuming that the cloud water content remained about the same, this would mean that the value for cwc/B varied between 0.5 and 10 times the estimated value of 23 gsr/m^2, i.e., between 11.5 and 230 gsr/m^2. Therefore the effective radii of the ice crystals estimated from Figure 5 ranges from 4 to 40 μm. This size range can be thought of as the uncertainty of the estimated radius (5 μm) caused by the horizontal separation of the observations by lidar and CFH.

4.2. Upper Limit of the Cloud Particle Size From Time Constants of Sedimentation and of Growth

[26] The time for condensational growth and sedimentation provide an upper limit for the cloud particle size, given the cwc given in section 4.1.

[27] The time t_d for a particle to grow to radius r is given by equation (A2) in Appendix A2. The observations indicate a lower limit for cwc of about 0.3 ppmv of water at 80 hPa (~17.5 km) (Figure 4). Since the vertical extent of the cirrus cloud was less than 1 km, the time t_s for sedimentation should not be more than the time it takes a cloud particle to fall 1 km, which would mean to fall out of the cloud layer, or

$$t_s = (1\ \text{km})/w, \tag{3}$$

where w is the sedimentation velocity described in Appendix A4.

[28] Figure 7 shows the growth time t_d, and the sedimentation time t_s as a function of effective radius. Both time constants intersect at a radius of about 15 μm. The signif-

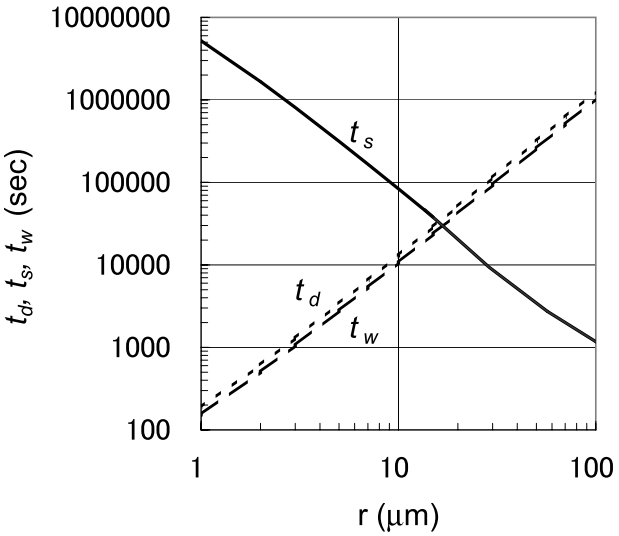

Figure 7. Calculated time constants (t_s, t_d, t_w) versus the radius. Solid line indicates t_s, dotted line indicates t_d, and dashed line indicates t_w.

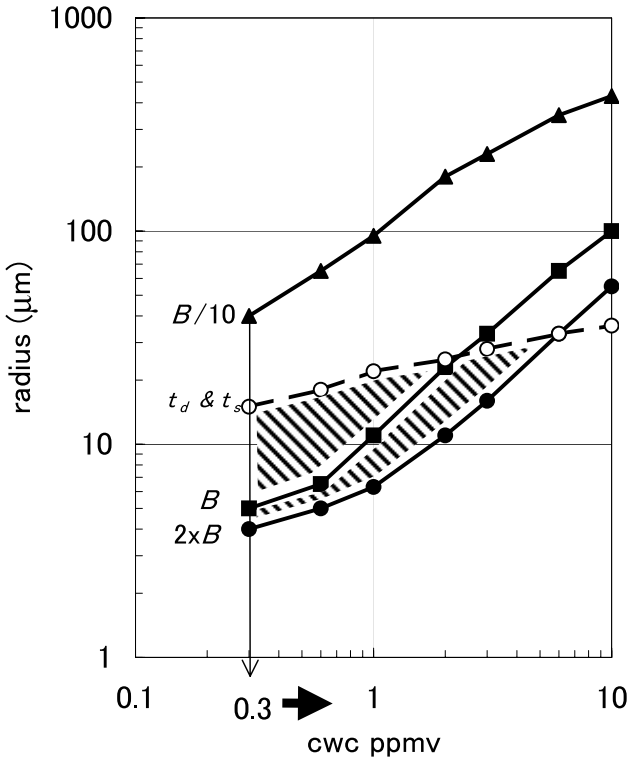

Figure 8. Estimated radii for assumed cwc: radius calculated by cwc/B using observed B (solid line with squares), by 0.5 × cwc/B using 2 × B (solid line with circle), and by 10 × cwc/B using B/10 (solid line with triangles). Also shown are the radius at the intersection of time constants t_d and t_s (dashed line with open circles) and the area (hatched) where the radii by cwc/B and by t_d and t_s. The value of cwc should be larger than 0.3 g/m^3 (thin and bold arrows).

icance of this intersection is that particles larger than about 15 μm would fall out of the cloud before they could grow to this size, which implies that the particles cannot grow much larger than this radius. The size range estimated here from t_d and t_s and the size range estimated in the previous section from cwc/B overlap between 4 and 15 μm.

[29] If there were strong vertical winds, the estimation described above would be invalid. The synoptic-scale vertical wind velocity given by NCEP reanalysis data (images (not shown here) from the Web site of NOAA at http://www.cdc.noaa.gov/ [*Kalnay et al.*, 1996]) indicate that there was a slight downward motion on the order of 0.1 cm/s at 100 hPa level over Bandung on the morning of 16 December 2004. This synoptic-scale velocity is small enough not to affect the above estimation. The weather satellite (GOES 9) images show that there were no clouds that indicated the existence of deep convection in the vicinity on that morning (images (not shown here) from the Web site of Kochi University at http://weather.is.kochi-u.ac.jp/).

4.3. Ranges of cwc and Particle Size Consistent With the Observations

[30] The true value of cwc may be larger than the lower limit of about 0.3 ppmv, which would increase the effective particle size in both methods of estimation. Figure 8 shows the relation between the cwc and the effective particle size calculated by both methods. For the calculations based on the backscatter coefficient (section 4.1), the particle size estimate is shown for the measured backscatter coefficient (square), as well as twice (solid circle) and one tenth (triangle) of the measured backscatter coefficient. This range for the backscatter coefficient provides a range for the lower limit of the particle size as a function of the cloud water content.

[31] The dashed line (open circle) indicates the largest radius particles may achieve before falling out of the cloud on the basis of the growth time and sedimentation time (section 4.2). The effective radius should be less than this estimate for any given cwc. Combining these two estimates would imply that for the observations presented here the mean effective particle radius should only fall in the hatched area. With these limits the effective particle size should range between 4 and 30 μm.

[32] Although the estimated cwc in the section 4.1 is only a lower limit, we can estimate an upper limit of cwc assuming that the size range estimates by the methods of sections 4.1 and 4.2 should overlap. In other words: given the observed value of B, if cwc had a larger value, the particle size would increase. Since the sedimentation velocity of the larger particles also increases, the upper limit of the size (or cwc) is given for particles that stay within the cloud layer. Figure 8 indicates that 6 ppmv is the upper limit for the cloud water content of the cirrus cloud observed by the lidar. The hatched area of Figure 8 indicates that the observations allow cloud water content between 0.3 and 6 ppmv, and a radius of cloud particles between 4 and 30 μm. This estimated radius is consistent with previous observations, e.g., *Gao et al.* [2004], *Peter et al.* [2003], or *Jensen et al.* [2005b], who reported size observations in the range of 5–40 μm.

4.4. Implications

[33] Sulfuric acid particles may be the main atmospheric aerosol particles in the tropical upper troposphere [*Brock et al.*, 1995; *Clarke and Kapustin*, 2002]. About 4 K of supercooling is required for the ice particles to form from sulfuric acid particles [*Koop et al.*, 1997, 1998]. This process could support significant supersaturation at the altitude where the clouds do not exist.

[34] The amount of water vapor that passes through the cold trap of the tropical tropopause into the lower stratosphere is usually estimated using the saturation vapor pressure at the altitude of the lowest temperature [e.g., *Newell and Gould-Stewart*, 1981; *Dessler*, 1998]. The supersaturation observed in this study indicates that supersaturation needs to be taken into account to estimate the water vapor transport from the troposphere to stratosphere [e.g., *Vömel and Oltmans*, 1999; *Jensen et al.*, 2001].

[35] *Gao et al.* [2004] proposed a mechanism for their observed supersaturation with cloud particles. Although supersaturation with cirrus cloud particles in a state of equilibrium can be achieved by their proposed mechanism, supersaturation can continue for hours, even where cirrus cloud particles exist without such a mechanism. The time constants for the water vapor (t_w) with cloud particles are shown in Figure 7 (dashed line). If the radius of the cloud particles is larger than several micrometers, t_w is in the order

of hours. Further evidence is needed to determine whether the supersaturation was observed in conditions of equilibrium.

[36] Since only few simultaneous observations of water vapor and cirrus clouds were obtained here, more observations of this kind are needed to establish a stronger observational basis for the dehydration processes in the cold pool over the maritime continent, but also in other regions, e.g., the Central American monsoon region during the boreal summer. Ideally, observations of cirrus clouds and water vapor should be obtained with minimal horizontal separation to estimate the value of cwc/B more accurately. Given the variability of tropospheric winds, observations with minimal separation are on occasion possible. In addition, in situ measurements of cloud particle size and shape as well as a direct measurement of the cloud water content in addition to lidar and CFH observations will improve the understanding of the nature of the tropical tropopause cirrus clouds.

[37] Until now, most observations of particle size in cirrus clouds have been obtained by airborne light scattering instruments like the FSSP (Forward Scattering Spectrometer Probe). However, these instruments generally need a heavy lift platform like an aircraft, and cannot provide shape information of the particles.

[38] Video particle sondes can detect cloud particles with sizes larger than several microns and can be launched using small balloons similar to those used for the CFH. Since video sondes record particle images, they also provide shape information. For particle sizes in the range of 4 to 30 μm, video particle sondes will be a most useful complement for the observations by balloon-borne CFH and ground based lidar, although the lower end of the estimated size range is near the limit of the video sonde. Multiwavelength depolarization lidar can provide size and shape information up to several micrometers [e.g., *Peter et al.*, 2003] and would be useful to take further size and shape information of the cirrus clouds. Additional observations of these kinds are planned to improve our understanding of the cloud processes in the tropical tropopause region.

5. Summary

[39] A few to several tens percent of supersaturation were observed by the Cryogenic Frost point Hygrometer (CFH) just below the tropopause in the same altitude range where the lidar observed thin cirrus clouds. Although the degree of supersaturation was similar to other studies [*Jensen et al.*, 1998; *Ovarlez et al.*, 2002; *Luo et al.*, 2003; *Gao et al.*, 2004; *Jensen et al.*, 2005a], a detailed relation between the vertical distributions of humidity and cirrus cloud was obtained for the first time using CFH and lidar observations. The vertical range of cirrus clouds and supersaturation did not coincide precisely. Supersaturation was observed over a vertical range larger than that of cirrus clouds. The humidity profile also showed fine structure within cirrus clouds, with a pronounced decreased in the altitude of the cirrus clouds while still remaining above saturation.

[40] Assuming that this water vapor decrease was due to uptake by cloud particles, the lidar observed backscattering coefficient, theoretical calculations of the scattering parameters for the cirrus cloud particles, and estimations of the time constant for sedimentation and condensational growth indicate that the particle size range is between 4 μm and 30 μm. Direct observations of cloud particles will improve the understanding of the nature of the tropical tropopause cirrus clouds.

Appendix A

A1. Light Scattering by Cirrus Cloud Particles

[41] The theoretical relation between cwc/B and cloud particle radius is obtained as follows: The cloud particles are about one to two orders of magnitude larger than the lidar wavelength and thus in the range of geometrical optics. We used theoretical results by *Hess et al.* [1998] to estimate the light scattering of the cirrus clouds and the relation between the size and cwc/B. Their calculations were made by geometrical ray tracing at several wavelengths for randomly oriented hexagonal ice column particles that have a given size and shape, and provide scattering parameters for these particles. The light scattering parameters are calculated at wavelengths of 355 and 550 nm [*Hess et al.*, 1998] using the following parameters for hexagonal crystals. For crystals size we use radii of 1.4, 4, 10, 22, 41, 60, 80, and 110 μm and for shape we use aspect ratios of 1.25, 1.25, 1.5, 1.4, 1.6, 2.5, 3.8, and 5.9 respectively, following the results by *Auer and Veal* [1970], where the aspect ratio is defined as c/2a and where a and c denote the radius and length of the crystal, respectively. For the values at the lidar wavelength of 532 nm the results from the two wavelengths used by *Hess et al.* [1998] are linearly interpolated.

[42] Although the relations between the size and cwc/B or N are calculated for the hexagonal columns with fixed aspect ratios, they are approximately applicable for particles whose relation between size and volume is similar. The relation will be useful at least for order estimations.

A2. Time Constant for Condensational Growth: t_d

[43] The rate of growth due to water vapor condensation is expressed as follows [*Hamill et al.*, 1977; *Pruppacher and Klett*, 1978; *Toon et al.*, 1989]:

$$\frac{dr}{dt} = \frac{vD(n_w - n_{w0})}{r(1 + \lambda Kn)}, \tag{A1}$$

where r is the particle radius, v is the volume per molecule in the particle, D is the diffusivity of water vapor, n_w and n_{w0} are the number densities of H_2O molecules in air and in saturated air, respectively, Kn is the Knudsen number defined as l/r(l is the mean free path), and λ is a correction factor. λ is expressed as

$$\lambda = \frac{1.333 + 0.71Kn^{-1}}{1 + Kn^{-1}} + \frac{4(1 - \alpha)}{3\alpha},$$

where α is the accommodation coefficient and assumed to be unity here. The time t_d for a particle to grow to radius r is obtained as

$$t_d = \frac{r^2(1 + \lambda Kn)}{2vD(n_w - n_{w0})}. \tag{A2}$$

The values of D and ν are calculated using the formulas by *Pruppacher and Klett* [1978]. If the ice is nucleated in the sulfuric acid droplet particles, estimated t_d is an overestimate of the growth time. However, since the radius of

sulfuric acid particles is in the sub micron range, the amount of overestimation will be negligible.

A3. Time Constant for Water Vapor: t_w

[44] The variation of water vapor concentration n_w by the condensation and evaporation of water molecules is estimated as follows [*Pruppacher and Klett*, 1978]:

$$\frac{dn_w}{dt} = -\frac{4\pi r D(n_w - n_{w0})n_r}{1 + \lambda Kn}. \quad \text{(A3)}$$

where r is the radius of condensing cloud particles, n_{w0} is saturation water vapor concentration, and n_r is the number concentration of cloud particles with radius r, respectively. From equation (A3) the time constant for the condensation of water vapor (exponential decay time of the water vapor concentration approaches steady state), t_w, is calculated as

$$t_w = \frac{1 + \lambda Kn}{4\pi r D n_r}. \quad \text{(A4)}$$

The time constant t_w was estimated for the cirrus clouds with single size particles, and was calculated for each cloud particle size of r. The number n_r was determined as the cloud particles by this size r only have water content of 0.43×10^{-10} g/cm^3. This value of cwc was obtained in section 4.1 by the ratio cwc/B = 23 gsr/m^2, and by the lidar observed B for the data in Figure 5.

A4. Time Constant for Sedimentation: t_s

[45] On the basis of the Reynolds number N_{Re}, there are two regimes of sedimentation of the particles in the atmosphere. In the first regime ($10^{-6} < N_{Re} < 0.01$; $0.5 < r < 10$ μm) where the viscous force is dominant, the sedimentation velocity is calculated using the Stokes-Cunningham equation. In the second regime ($10^{-2} < N_{Re} < 300$; $10 < r < 535$ μm) where both the inertial and viscous forces are significant, the velocity is calculated using the Best number expression explained by *Pruppacher and Klett* [1978].

[46] In the first regime ($0.5 < r < 10$ μm), the sedimentation velocity w of spherical particles of radius r is expressed as

$$w = (2/9)\left(\rho_p r^2 g/\eta\right)[1 + (l/r)(A + B\exp\{-Cr/l\})], \quad \text{(A5)}$$

where ρ_p is the density of the particles, g is the acceleration of gravity, η is the dynamic viscosity, l is the mean free path, and A, B, and C are the constants described by *Kasten* [1968]. The settling velocity of aspherical particles like cirrus cloud particles is expressed by equation (A3) divided by the dynamic shape factor [*Fuchs*, 1964]. We determined this factor as the velocity calculated from equation (A3) approaches the value of the velocity calculated for the second regime at a radius of about 15 μm.

[47] In the second regime ($10 < r < 535$ μm), the Best number is calculated using radius and length of a hexagonal particle, the density of the particle, and the dynamic viscosity. The Reynolds number is then calculated using the empirical expressions of the Reynolds number as function of the Best number corresponding to three aspect ratios of hexagonal ice crystals [*Pruppacher and Klett*, 1978]. The settling velocity w is calculated from the Reynolds number. The calculations are done for the three provided aspect ratios of 1, 2, and 10. The velocity w for these aspect ratios is calculated and interpolated for the aspect ratio at each radius of the hexagonal crystals mentioned in section 4.1.

[48] **Acknowledgments.** This work was supported by Japan Society for the Promotion of Science, Grant-in-Aid for Scientific Research (A) 15204043, and was also supported by the Ministry of Education, Culture, Sports, Science and Technology, Japan, for the 21st Century COE Program (Dynamics of the Sun-Earth-Life Interactive System, G-4). NCEP reanalysis data images were provided by the NOAA-CIRES Climate Diagnostics Center, Boulder, Colorado, from their web site at http://www.cdc.noaa.gov/. The weather satellite (GOES 9) images were provided by T. Kikuchi, Kochi University, from the Web site at http://weather.is.kochi-u.ac.jp/.

References

Attics, M. G., and G. D. Robinson (1983), Some features of the structure of the tropical tropopause, *Q. J. R. Meteorol. Soc.*, *109*, 295–308.

Auer, A. H., and D. L. Veal (1970), The dimension of ice crystals in natural clouds, *J. Atmos. Sci.*, *27*, 919–926.

Boehm, M. T., J. Verlinde, and T. P. Ackerman (1999), On the maintenance of high tropical cirrus, *J. Geophys. Res.*, *104*, 24,423–24,433.

Brock, C. A., P. Hamill, J. C. Wilson, H. H. Jonsson, and K. R. Chan (1995), Particle formation in the upper tropical troposphere: A source of nuclei for the stratospheric aerosol, *Science*, *270*, 1650–1653.

Clarke, A. D., and V. N. Kapustin (2002), A Pacific aerosol survey. Part I: A decade of data on particle production, transport, evolution, and mixing in the troposphere, *J. Atmos. Sci.*, *59*, 363–382.

Corti, T., B. P. Luo, Q. Fu, H. Vömel, and T. Peter (2006), The impact of cirrus clouds on tropical troposphere-to-stratosphere transport, *Atmos. Chem. Phys. Discuss.*, *6*, 1725–1747.

Dessler, A. E. (1998), A reexamination of the "stratospheric fountain" hypothesis, *Geophys. Res. Lett.*, *25*, 4165–4168.

Dessler, A. E., S. P. Palm, W. D. Hart, and J. D. Spinhirne (2006), Tropopause-level thin cirrus coverage revealed by ICESat/Geoscience Laser Altimeter System, *J. Geophys. Res.*, *111*, D08203, doi:10.1029/2005JD006586.

Folkins, I., M. Loewenstein, J. Podolske, S. J. Oltmans, and M. Proffitt (1999), A barrier to vertical mixing at 14 km in the tropics: Evidence from ozonesondes and aircraft measurements, *J. Geophys. Res.*, *104*, 22,095–22,102.

Fuchs, N. A. (1964), *The Mechanics of Aerosols*, Elsevier, New York.

Gao, R. S., et al. (2004), Evidence that nitric acid increases relative humidity in low-temperature cirrus clouds, *Science*, *303*, 516–520.

Gierens, K., U. Schumann, M. Helten, H. Smit, and P. H. Wang (2000), Ice-supersaturated regions and subvisible cirrus in the northern midlatitude upper troposphere, *J. Geophys. Res.*, *105*, 22,743–22,753.

Goff, J. A., and S. Gratch (1946), Low-pressure properties of water from −160 to 212 F, *Trans. Am. Soc. Heat. Ventilating Eng.*, *52*, 95–122.

Hamill, P., O. B. Toon, and C. S. Kiang (1977), Microphysical processes affecting stratospheric aerosol particles, *J. Atmos. Sci.*, *34*, 1104–1119.

Hess, H., R. B. A. Koelemeijer, and P. Stammes (1998), Scattering matrices of impaerfect hexagonal ice crystals, *J. Quant. Spectrosc. Radiat. Transfer*, *60*, 301–308.

Highwood, E. J., and B. J. Hoskins (1998), The tropical tropopause, *Q. J. R. Meteorol. Soc.*, *124*, 1579–1604.

Holton, J. R., and A. Gettelman (2001), Horizontal transport and the dehydration of the stratosphere, *Geophys. Res. Lett.*, *28*, 2799–2802.

Jensen, E. J., O. B. Toon, L. Pfister, and H. B. Selkirk (1996a), Dehydration of the upper troposphere and lower stratosphere by subvisible cirrus clouds near the tropical tropopause, *Geophys. Res. Lett.*, *23*, 825–828.

Jensen, E. J., O. B. Toon, H. B. Selkirk, J. D. Spinhirne, and M. R. Schoeberl (1996b), On the formation and persistence of subvisible cirrus clouds near the tropical tropopause, *J. Geophys. Res.*, *101*, 21,361–21,375.

Jensen, E. J., et al. (1998), Ice nucleation processes in upper tropospheric wave-clouds observed during SUCCCESS, *Geophys. Res. Lett.*, *25*, 1363–1366.

Jensen, E. J., W. G. Read, J. Mergenthaler, B. J. Sandor, L. Pfister, and A. Tabazadeh (1999), High humidities and subvisible cirrus near the tropical tropopause, *Geophys. Res. Lett.*, *26*, 2347–2350.

Jensen, E. J., O. B. Toon, S. A. Vay, J. Ovarlez, R. May, T. P. Bui, C. H. Twohy, B. W. Gandrud, R. F. Pueschel, and U. Schumann (2001), Prevalence of ice-supersaturated regions in the upper troposphere: Implications for optically thin ice cloud formation, *J. Geophys. Res.*, *106*, 17,253–17,266.

Jensen, E., et al. (2005a), Ice supersaturations exceeding 100% at the cold tropical tropopause: Implications for cirrus formation and dehydration, *Atmos. Chem. Phys.*, *5*, 851–862.

Jensen, E., L. Pfister, T. Bui, A. Weinheimer, E. Weinstock, J. Smith, J. Pittman, D. Baumgardner, P. Lawson, and M. J. McGill (2005b), Formation of a tropopause cirrus layer observed over Florida during CRYSTAL-FACE, *J. Geophys. Res.*, *110*, D03208, doi:10.1029/2004JD004671.

Kalnay, E., et al. (1996), The NCEP/NCAR Reanalysis 40-year Project, *Bull. Am. Meteorol. Soc.*, *77*, 437–471.

Kasten, F. (1968), Falling speed of aerosol particles, *J. Appl. Meteorol.*, *7*, 944–947.

Koop, T., B. P. Luo, U. M. Biermann, P. J. Crutzen, and T. Peter (1997), Freezing of $HNO_3/H_2SO_4/H_2O$ solutions at stratospheric temperatures: Nucleation statistics and experiments, *J. Phys. Chem. A*, *101*, 1117–1133.

Koop, T., H. P. Ng, L. T. Molina, and M. J. Molina (1998), A new optical technique to study aerosol phase transitions: The nucleation of ice from H_2SO_4 aerosols, *J. Phys. Chem. A.*, *102*, 8924–8931.

Koop, T., B. Luo, A. Tsias, and T. Peter (2000), Water activity as the determinant for homogeneous ice nucleation in aqueous solution, *Nature*, *406*, 611–614.

Lynch, D. K., and K. Sassen (2002), Subvisual cirrus, in *Cirrus*, edited by D. K. Lynch et al., pp. 256–264, Oxford Univ. Press, New York.

Luo, B. P., et al. (2003), Ultrathin tropical tropopause clouds (UTTCs): II. Stabilization mechanisms, *Atmos. Chem. Phys.*, *3*, 1093–1100.

Murphy, D. M. (2005), Commentary on "Measurements of ice supersaturations exceeding 100% at the cold tropical tropopause" by E. Jensen et al., *Atmos. Chem. Phys. Discuss.*, *5*, 2463–2468.

Newell, R. E., and S. Gould-Stewart (1981), A stratospheric fountain?, *J. Atmos. Sci.*, *38*, 2789–2796.

Ovarlez, J., J. Gayet, K. Gierens, J. Ström, H. Ovarlez, F. Auriol, R. Busen, and U. Schumann (2002), Water vapour measurements inside cirrus clouds in northern and southern hemispheres during INCA, *Geophys. Res. Lett.*, *29*(16), 1813, doi:10.1029/2001GL014440.

Peter, T., et al. (2003), Ultrathin tropical tropopause clouds (UTTCs): I. cloud morphology and occurrence, *Atmos. Chem. Phys.*, *3*, 1083–1091.

Pruppacher, H. R., and J. D. Klett (1978), *Microphysics of Clouds and Precipitation*, Springer, New York.

Rosenfield, J. E., D. B. Considine, M. R. Schoeberl, and E. V. Browell (1998), The impact of subvisible cirrus clouds near the tropical tropopause on stratospheric water vapor, *Geophys. Res. Lett.*, *25*, 1883–1886.

Toon, O. B., R. P. Turco, J. Jordan, J. Goodman, and G. Ferry (1989), Physical processes in polar stratospheric ice clouds, *J. Geophys. Res.*, *94*, 11,359–11,380.

Vömel, H., and S. J. Oltmans (1999), Comment on "A reexamination of the 'stratospheric fountain' hypothesis" by A. E. Dessler, *Geophys. Res. Lett.*, *26*, 2737–2738.

Vömel, H., S. J. Oltmans, D. J. Hofmann, T. Deshler, and J. M. Rosen (1995), The evolution of the dehydration in the Antarctic stratospheric vortex, *J. Geophys. Res.*, *100*, 13,919–13,926.

Vömel, H., et al. (2002), Balloon-borne observations of water vapor and ozone in the tropical upper troposphere and lower stratosphere, *J. Geophys. Res.*, *107*(D14), 4210, doi:10.1029/2001JD000707.

Vömel, H., D. David, and K. Smith (2006), Accuracy of tropospheric and stratospheric water vapor measurements by the Cryogenic Frost Point Hygrometer (CFH): Instrumental details and observations, *J. Geophys. Res.*, doi:10.1029/2006JD007224, in press.

Wang, P. H., P. Minnis, M. P. McCormick, G. S. Kent, and K. M. Skeens (1996), A 6-year climatology of cloud occurrence frequency from stratospheric aerosol and gas experiment: II. Observations (1985–1990), *J. Geophys. Res.*, *101*, 29,407–29,429.

Winker, D. M., and C. R. Trepte (1998), Laminar cirrus observed near tropical tropopause by LITE, *Geophys. Res. Lett.*, *25*, 3351–3354.

M. Fujiwara and F. Hasebe, Faculty of Environmental Earth Science, Hokkaido University, Sapporo 060-0810, Japan.

S. Hamdi and S. Kaloka, Lembaga Penerbangan dan Antariksa Nasional, Bandung 40173, Indonesia.

T. Shibata, Graduate School of Environmental Studies, Nagoya University, Nagoya 464-8601, Japan. (tshibata@stelab.nagoya-u.ac.jp)

M. Shiotani, Research Institute for Sustainable Humanosphere, Kyoto University, Kyoto 611-0011, Japan.

H. Vömel, Cooperative Institute for Research in Environmental Sciences, University of Colorado, Boulder, CO 80309, USA.